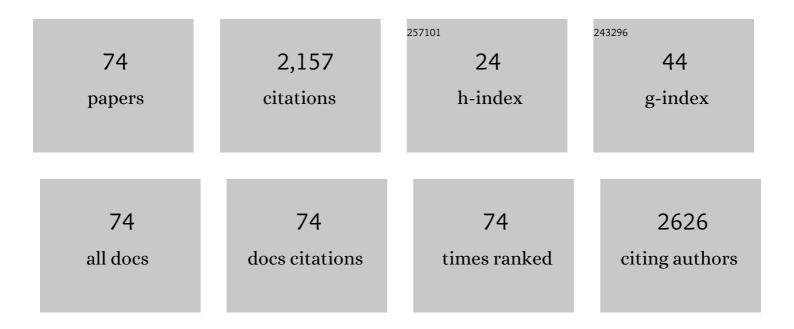
Daoli Zhang

List of Publications by Year in descending order

Source: https://exaly.com/author-pdf/7490103/publications.pdf Version: 2024-02-01



#	Article	IF	CITATIONS
1	Single omponent White‣ight Emitters with Excellent Color Rendering Indexes and High Photoluminescence Quantum Efficiencies. Advanced Optical Materials, 2022, 10, .	3.6	18
2	Directional etching for high aspect ratio nano-trenches on hexagonal boron nitride by catalytic metal particles. 2D Materials, 2022, 9, 025015.	2.0	8
3	Efficient Enhancement of Stability and Luminescence of Three-Dimensional CsPbBr ₃ Nanoparticles via Ligand-Triggered Transformation into Zero-Dimensional Cs ₄ PbBr ₆ Nanoparticles. Journal of Physical Chemistry C, 2022, 126, 4172-4181.	1.5	4
4	Highly luminescent zero-dimensional lead-free manganese halides for Î ² -ray scintillation. Nano Research, 2022, 15, 8486-8492.	5.8	18
5	Highly Luminescent Zero-Dimensional Organic Copper Halide with Low-Loss Optical Waveguides and Highly Polarized Emission. , 2022, 4, 1446-1452.		21
6	Efficient Infrared Solar Cells Employing Quantum Dot Solids with Strong Interâ€Dot Coupling and Efficient Passivation. Advanced Functional Materials, 2021, 31, 2006864.	7.8	16
7	Towards chirality control of graphene nanoribbons embedded in hexagonal boron nitride. Nature Materials, 2021, 20, 202-207.	13.3	80
8	Enhanced Photoluminescence of Colloidal Leadâ€Free Double Perovskite Cs ₂ Ag _{1â^'} <i>_x</i> Na <i>_x</i> InCl ₆ Nanocrystals Doped with Manganese. Advanced Optical Materials, 2021, 9, 2001866.	3.6	24
9	Efficient Dual-Band White-Light Emission with High Color Rendering from Zero-Dimensional Organic Copper Iodide. ACS Applied Materials & Interfaces, 2021, 13, 22749-22756.	4.0	57
10	Synthesis of Highly Luminescent InP/ZnS Quantum Dots with Suppressed Thermal Quenching. Coatings, 2021, 11, 581.	1.2	4
11	Highly Luminescent Zero-Dimensional Organic Copper Halides for X-ray Scintillation. Journal of Physical Chemistry Letters, 2021, 12, 6919-6926.	2.1	95
12	Efficiently Passivated PbSe Quantum Dot Solids for Infrared Photovoltaics. ACS Nano, 2021, 15, 3376-3386.	7.3	32
13	Realizing Near-Unity Quantum Efficiency of Zero-Dimensional Antimony Halides through Metal Halide Structural Modulation. ACS Applied Materials & Interfaces, 2021, 13, 58908-58915.	4.0	36
14	Cationâ€Exchange Synthesis of Highly Monodisperse PbS Quantum Dots from ZnS Nanorods for Efficient Infrared Solar Cells. Advanced Functional Materials, 2020, 30, 1907379.	7.8	80
15	Nonvolatile Resistive Switching Memory Device Employing CdSe/CdS Core/Shell Quantum Dots as an Electrode Modification Layer. ACS Applied Electronic Materials, 2020, 2, 827-837.	2.0	15
16	Photophysics in Cs ₃ Cu ₂ X ₅ (X = Cl, Br, or I): Highly Luminescent Self-Trapped Excitons from Local Structure Symmetrization. Chemistry of Materials, 2020, 32, 3462-3468.	3.2	177
17	Facet Control for Trapâ€5tate Suppression in Colloidal Quantum Dot Solids. Advanced Functional Materials, 2020, 30, 2000594.	7.8	60
18	Efficient and Reabsorptionâ€Free Radioluminescence in Cs ₃ Cu ₂ I ₅ Nanocrystals with Selfâ€Trapped Excitons. Advanced Science, 2020, 7, 2000195.	5.6	282

Daoli Zhang

#	Article	IF	CITATIONS
19	Isolating hydrogen in hexagonal boron nitride bubbles by a plasma treatment. Nature Communications, 2019, 10, 2815.	5.8	63
20	Controlled synthesis and photostability of blue emitting Cs ₃ Bi ₂ Br ₉ perovskite nanocrystals by employing weak polar solvents at room temperature. Journal of Materials Chemistry C, 2019, 7, 3688-3695.	2.7	50
21	Dependence of the Photoluminescence of Hydrophilic CuInS2 Colloidal Quantum Dots on Cu-to-In Molar Ratios. Journal of Electronic Materials, 2019, 48, 286-295.	1.0	5
22	Phosphine-free synthesis and shape evolution of MoSe ₂ nanoflowers for electrocatalytic hydrogen evolution reactions. CrystEngComm, 2018, 20, 2491-2498.	1.3	21
23	Self-assembly and photoactivation of blue luminescent CsPbBr ₃ mesocrystals synthesized at ambient temperature. Journal of Materials Chemistry C, 2018, 6, 1701-1708.	2.7	17
24	In Situ Tuning the Reactivity of Selenium Precursor To Synthesize Wide Range Size, Ultralarge-Scale, and Ultrastable PbSe Quantum Dots. Chemistry of Materials, 2018, 30, 982-989.	3.2	27
25	Controlled synthesis of brightly fluorescent CH ₃ NH ₃ PbBr ₃ perovskite nanocrystals employing Pb(C ₁₇ H ₃₃ COO) ₂ as the sole lead source. RSC Advances, 2018, 8, 1132-1139.	1.7	6
26	Phosphine-free synthesis and optical stabilities of composition-tuneable monodisperse ternary PbSe _{1â^x} S _x alloyed nanocrystals <i>via</i> cation exchange. CrystEngComm, 2018, 20, 2519-2527.	1.3	3
27	Colloidal synthesis of lead-free all-inorganic cesium bismuth bromide perovskite nanoplatelets. CrystEngComm, 2018, 20, 7473-7478.	1.3	44
28	Electron Beam Induced Formation of Hollow RbBr Nanocubes. Journal of Physical Chemistry C, 2018, 122, 28347-28350.	1.5	0
29	Solution-processed solar-blind deep ultraviolet photodetectors based on strongly quantum confined ZnS quantum dots. Journal of Materials Chemistry C, 2018, 6, 11266-11271.	2.7	46
30	Transparent Thin-Film Transistors Based on c-Axis Oriented, Vertically Aligned ZnO Nanorod Arrays via Solution Processing. Journal of Electronic Materials, 2018, 47, 6091-6100.	1.0	0
31	Low cost and large scale synthesis of PbS quantum dots with hybrid surface passivation. CrystEngComm, 2017, 19, 946-951.	1.3	24
32	Oriented graphene nanoribbons embedded in hexagonal boron nitride trenches. Nature Communications, 2017, 8, 14703.	5.8	119
33	Combination of Cation Exchange and Quantized Ostwald Ripening for Controlling Size Distribution of Lead Chalcogenide Quantum Dots. Chemistry of Materials, 2017, 29, 3615-3622.	3.2	44
34	Dynamics of graded-composition and graded-doping semiconductor nanowires under local carrier modulation. Optics Express, 2016, 24, 24347.	1.7	0
35	Resolution characteristics of graded band-gap reflection-mode AlGaAs/GaAs photocathodes. Optics Communications, 2015, 356, 278-281.	1.0	3
36	Phosphorus-doping-induced rectifying behavior in armchair graphene nanoribbons devices. Journal of Applied Physics, 2014, 115, .	1.1	18

DAOLI ZHANG

#	Article	IF	CITATIONS
37	Metallic behavior and negative differential resistance properties of (InAs)n(n = 2 â~` 4) molecule junctionsviaa combined non–equilibrium Green's function and density functional theory study. Journal of Applied Physics, 2014, 115, 233712.	cluster 1.1	2
38	The electronic transport behavior of hybridized zigzag graphene and boron nitride nanoribbons. Journal of Applied Physics, 2014, 115, .	1.1	18
39	Negative differential resistance behavior in phosphorus-doped armchair graphene nanoribbon junctions. Journal of Applied Physics, 2014, 115, .	1.1	26
40	Temporal evolutions of the photoluminescence quantum yields of colloidal InP, InAs and their core/shell nanocrystals. Journal of Materials Chemistry C, 2014, 2, 4442-4448.	2.7	8
41	Electronic transport behaviours of lead chalcogenide (PbE)n (E = S and Se) nanocluster junctions by ab initio simulation. RSC Advances, 2014, 4, 14221-14226.	1.7	2
42	One-pot synthesis of hydrophilic CuInS ₂ and CuInS ₂ –ZnS colloidal quantum dots. Journal of Materials Chemistry C, 2014, 2, 4812-4817.	2.7	43
43	A facile and rapid synthesis of lead sulfide colloidal quantum dots using in situ generated H2S as the sulfur source. CrystEngComm, 2013, 15, 2532.	1.3	20
44	Thermal Properties of TiO ₂ /PbS Nanoparticle Solar Cells. Nanomaterials and Nanotechnology, 2012, 2, 18.	1.2	2
45	nanocluster-based molecular junctions. Physics Letters, Section A: General, Atomic and Solid State		17
46	Nysics, 2012, 576, 5272-5276. Quantum dot PbS _{0.9} Se _{0.1} /TiO ₂ heterojunction solar cells. Nanotechnology, 2012, 23, 405401.	1.3	31
47	Optical and electrical properties of zinc oxide thin films with low resistivity via Li–N dual-acceptor doping. Journal of Alloys and Compounds, 2011, 509, 5962-5968.	2.8	22
48	Theoretical Investigation of Structural and Magnetic Properties of Zn _{<i>n</i>} Se _{<i>n</i>} (<i>n</i> =6–13) Nanoclusters Doped with Manganese Atoms. Journal of the American Ceramic Society, 2011, 94, 759-764.	1.9	7
49	Investigation into Texture, Preferential Orientation, and Optical Properties of Zinc Oxide Nanopolycrystalline Thin Films Deposited by the Sol–Gel Technique on Different Substrates. Journal of Electronic Materials, 2011, 40, 459-465.	1.0	3
50	Air stability of TiO2/PbS colloidal nanoparticle solar cells and its impact on power efficiency. Applied Physics Letters, 2011, 99, 063512.	1.5	29
51	Ultraviolet emission of ZnO nano-polycrystalline films by modified successive ionic layer adsorption and reaction technique. Journal of Sol-Gel Science and Technology, 2010, 54, 165-173.	1.1	9
52	Comparative study of ZnSe thin films deposited from modified chemical bath solutions with ammonia-containing and ammonia-free precursors. Materials Chemistry and Physics, 2010, 120, 456-460.	2.0	34
53	Microstructure, Morphology, and Ultraviolet Emission of Zinc Oxide Nanopolycrystalline Films by the Modified Successive Ionic Layer Adsorption and Reaction Method. Journal of the American Ceramic Society, 2010, 93, 3284-3290.	1.9	17
54	Ultraviolet Emission and Electrical Properties of Aluminumâ€Doped Zinc Oxide Thin Films with Preferential <i>C</i> â€Axis Orientation. Journal of the American Ceramic Society, 2010, 93, 3291-3298.	1.9	9

DAOLI ZHANG

#	Article	IF	CITATIONS
55	Photoluminescence and Growth Kinetics of High-Quality Indium Arsenide and InAs-Based Core/Shell Colloidal Nanocrystals Synthesized Using Arsine (AsH ₃) Generated via Zinc Arsenide as the Arsenic Source. Chemistry of Materials, 2010, 22, 1579-1584.	3.2	19
56	Synthesis and growth kinetics of high quality InAs nanocrystals using in situ generated AsH ₃ as the arsenic source. CrystEngComm, 2010, 12, 591-594.	1.3	14
57	Growth orientation and shape evolution of colloidal lead selenide nanocrystals with different shapes. CrystEngComm, 2010, 12, 3243.	1.3	11
58	Synthesis and studies of spindle-shaped lead selenide nanocrystals. , 2009, , .		0
59	The growth kinetics of colloidal InP nanocrystals. , 2008, , .		0
60	Microstructure and electrical properties of antimony-doped tin oxide thin film deposited by sol–gel process. Materials Chemistry and Physics, 2006, 98, 353-357.	2.0	61
61	Surface morphologies and properties of pure and antimony-doped tin oxide films derived by sol–gel dip-coating processing. Materials Chemistry and Physics, 2006, 100, 275-280.	2.0	53
62	Effects of porosity on the electrical characteristics of current-limiting BaTiO3-based positive-temperature-coefficient (PTC) ceramic thermistors coated with electroless nickel–phosphorous electrode. Sensors and Actuators A: Physical, 2004, 112, 94-100.	2.0	17
63	Fabrication and characterization of the multilayered PTCR ceramic thermistors by slip casting. Sensors and Actuators A: Physical, 2004, 116, 450-454.	2.0	17
64	Influence of ZrO2 and SnO2 on the synthesis of Ba2Ti9O20 powders. Ceramics International, 2004, 30, 671-673.	2.3	1
65	The kinetics of initial stage in sintering process of BaTiO3-based PTCR ceramics and its computer simulation. Materials Science and Engineering B: Solid-State Materials for Advanced Technology, 2003, 99, 88-92.	1.7	9
66	Computer simulation of grain growth of intermediate—and final-stage sintering and Ostwald ripening of BaTiO3-based PTCR ceramics. Materials Science and Engineering B: Solid-State Materials for Advanced Technology, 2003, 99, 428-432.	1.7	12
67	Low-temperature sintering and microwave dielectric properties of (Zr,Sn)TiO4 ceramics. Materials Science and Engineering B: Solid-State Materials for Advanced Technology, 2003, 99, 416-420.	1.7	24
68	A new method for microwave dielectric measurement of low loss ceramics. Materials Science and Engineering B: Solid-State Materials for Advanced Technology, 2003, 99, 390-393.	1.7	9
69	Analysis on the aging characteristics of PTCR of donor-doped barium titanate. Materials Science and Engineering B: Solid-State Materials for Advanced Technology, 2003, 99, 394-398.	1.7	14
70	Microwave dielectric properties of (PbCa)(FeNbZr)O3 ceramics. Materials Science and Engineering B: Solid-State Materials for Advanced Technology, 2003, 99, 403-407.	1.7	15
71	Preparation and characteristic of the thermistor materials in the thick-film integrated temperature–humidity sensor. Materials Science and Engineering B: Solid-State Materials for Advanced Technology, 2003, 99, 523-526.	1.7	40
72	The ac electrical failure behaviors and mechanisms of current limiting BaTiO3-based positive-temperature-coefficient (PTC) ceramic thermistors coated with electroless nickel–phosphorous electrode. Sensors and Actuators A: Physical, 2002, 101, 123-131.	2.0	6

#	Article	IF	CITATIONS
73	PTCR characteristic of gelcast BaTiO3 ceramic thermistor. Sensors and Actuators A: Physical, 2001, 88, 67-70.	2.0	14
74	Influences of the electroless nickel electrode on the electrical characteristics of BaTiO3-based PTCR ceramics. Journal of the European Ceramic Society, 2001, 21, 1101-1105.	2.8	5